HHS Public Access

Author manuscript

Nat Chem. Author manuscript; available in PMC 2020 April 28.

Published in final edited form as:

Nat Chem. 2019 December ; 11(12): 1124–1132. doi:10.1038/s41557-019-0352-4.

Tailored Silyl Ether Monomers Enable Backbone-Degradable Polynorbornene-Based Linear, Bottlebrush, and Star Copolymers through ROMP

Peyton Shieh[1], **Hung V.-T. Nguyen**[1], **Jeremiah A. Johnson**[1,*]

[1]Department of Chemistry, Massachusetts Institute of Technology, 77 Massachusetts Avenue, Cambridge, MA 02139, United States

Abstract

Ring-opening metathesis polymerization (ROMP) of norbornene-based (macro)monomers is a powerful approach for the synthesis of macromolecules with diverse compositions and complex architectures. Nevertheless, a fundamental limitation of polymers prepared via this strategy is their lack of facile degradability, which limits their utility in a range of applications. Here, we describe a class of readily available bifunctional silyl-ether-based cyclic olefins that copolymerize efficiently with norbornene-based (macro)monomers to provide copolymers with backbone degradability under mildly acidic aqueous conditions and degradation rates that can be tuned over several orders-of-magnitude depending on the silyl ether substituents. These monomers can be used to manipulate the in vivo biodistribution and clearance rate of PEG-based bottlebrush polymers, as well as to synthesise linear, bottlebrush, and brush-arm star copolymers with degradable segments. We expect that this work will enable preparation of degradable polymers by ROMP for biomedical applications, responsive self-assembly, and improved sustainability.

Graphical abstract

*Correspondence to: jaj2109@mit.edu.

Author contributions

P.S. and J.A.J. conceived the idea. P.S. conducted all synthesis and characterization studies. P.S. and H.V.-T.N. conducted cell culture and *in vivo* studies. P.S. and J.A.J. wrote the manuscript. All authors discussed the results and commented on the manuscript.

Data availability

All data supporting the findings of this study are available within the Article and its Supplementary Information, and/or from the corresponding author upon reasonable request.

Competing interests

P.S. and J.A.J. are named inventors on a patent application filed by the Massachusetts Institute of Technology on the monomers and copolymers described in this work.

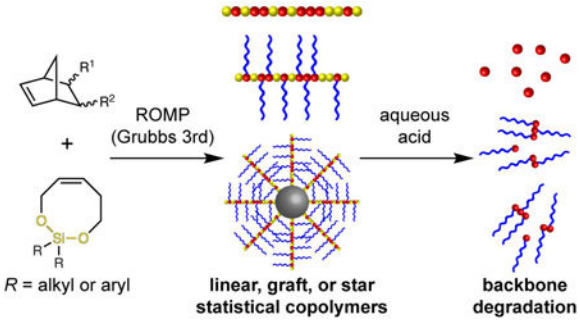

Given its mild-conditions, living nature, and exceptional functional group tolerance, ROMP of norbornene-based compounds has been widely used to generate functional materials for applications including resin technologies, biomedicine, catalysis, and sensing.[1–7] In addition, “graft-through” ROMP of norbornene-based macromonomers (MMs) that carry drug molecules, imaging agents, or diverse polymer sidechains has enabled rapid access to advanced polymer architectures for combination drug delivery, molecular imaging, and self-assembly.[8–16] Nevertheless, the lack of facile degradability of polynorbornene-based polymers is a key limitation (Figure 1a). For example, brush-arm star polymers (BASPs) prepared via ROMP of a norbornene-terminated polyethylene glycol (PEG) MM conjugated to the angiotensin receptor blocker telmisartan displayed *in vivo* persistence over several months.[17] It would be ideal to impart facile and tunable degradability into this important class of polymers without otherwise sacrificing their performance. Multiple examples of degradable ROMP polymers prepared via the use of non-norbornene-based monomers have been reported.[18–21] Though elegant, these monomers sometimes require lengthy syntheses; they display limited copolymerization efficiency with norbornene derivatives; or the polymers they produce are degradable only under forcing conditions. In addition, one example of a copolymer of norbornene and an oxadiazinone was reported to display sluggish hydrolysis under aqueous conditions, even at pH 1.[20] A straightforward approach to well-defined backbone-degradable co-polymers of norbornene-based (macro)monomers would significantly expand the functional scope of materials prepared by ROMP and, combined with the advent of catalytic ROMP, could make ROMP the go-to choice for the synthesis of advanced materials.[22]

Here, a class of bifunctional silyl-ether-based cyclic olefins that offers a general solution to this problem is described (Figure 1b). These monomers copolymerize with a variety of norbornene derivatives including small molecules and MMs, enabling the formation of backbone-degradable copolymers with controlled sizes, narrow molar mass distributions, and varied architecture (linear, bottlebrush, and BASP). Depending on the choice of silyl-ether substituents used, the degradation kinetics of the resulting copolymers can be tuned over several orders-of-magnitude. In addition, by simply adding a bifunctional silyl ether-based monomer during one step of a sequential copolymerization, block copolymers with selectively degradable segments can be readily formed. Finally, PEG-based bottlebrush polymers with degradable backbones are shown to be biocompatible and to display long-term *in vivo* biodistribution (BD) and clearance profiles that are distinct from their non-degradable counterparts.

Results and Discussion

Design of Bifunctional Silyl Ether Monomers for Backbone Degradable ROMP Copolymers

Given the precedence for using bifunctional silyl ethers as cleavable linkers in biological/biomaterials applications,[23,24] we chose to explore bifunctional silyl-ether-containing cyclic olefins as monomers to potentially introduce hydrolytically labile backbones into ROMP-derived polymers. A small set of bifunctional silyl-ether-based monomers, including rings of various sizes and *cis* versus *trans* olefins, was screened in a search for candidates that could copolymerize with norbornene-terminated 3.2 kDa **PEG-MM**.[12] Gratifyingly, when the relatively easy-to-synthesize (five steps in 14% overall yield on the 1 g scale from commercially available materials) eight-membered ring **iPrSi** (Figure 1c) was mixed with **PEG-MM** in a 1:1 molar ratio and exposed to 0.01 equivalents (total target DP 200) of 3rd-generation Grubbs bispyridyl complex (**G3**) for 30 minutes, gel permeation chromatography (GPC) of the reaction mixture revealed the presence of a new polymer, **iPrSi$_{100}$-PEG$_{100}$** (Figure 1d, blue trace), with low dispersity ($Đ$ = 1.14) and a slightly shorter retention time to that of an analogous DP = 100 bottlebrush polymer prepared using **PEG-MM** alone (**PEG$_{100}$**, Figure 1d, black trace). ^{1}H NMR spectroscopy confirmed the high conversion of **iPrSi** and **PEG-MM** (Supplementary Figure 1); thus, unless these two monomers completely homopolymerize, they must have formed a copolymer.

To preliminarily assess whether or not **iPrSi$_{100}$-PEG$_{100}$** is a statistical copolymer rather than a block copolymer, we exposed the polymerization reaction mixture to 0.2 M HCl in 10:1 dioxane/water and analyzed the resulting products by GPC. As expected for a statistical copolymer, **iPrSi$_{100}$-PEG$_{100}$** degraded (Figure 1d, blue dashed trace) into various lower mass species including identifiable one-, two-, and three-repeat-unit fragments (as determined by comparison to an independently prepared sample with target DP = 2, Supplementary Figure 2). In contrast, the homopolymer **PEG$_{100}$** did not degrade under these conditions (Figure 1d, black dashed trace). Analogous bottlebrush copolymers with target DPs of 20 (**iPrSi$_{10}$-PEG$_{10}$**) and 60 (**iPrSi$_{30}$-PEG$_{30}$**) yielded degradation products of similar size (Supplementary Figure 3), suggesting that the copolymerization of **iPrSi** and **PEG-MM** is efficient regardless of the target DP. In addition, MMs based on polylactic acid (**PLA-MM**), polystyrene (**PS-MM**)[25,26] (Supplementary Figure 4), and a drug (telmisartan) conjugate[27] (Supplementary Figure 5) could be used in the same manner to produce backbone degradable bottlebrush copolymers with PLA (**iPrSi$_{30}$-PLA$_{30}$**), PS (**iPrSi$_{30}$-PS$_{30}$**), and PEG-*branch*-drug-conjugated sidechains (**iPrSi$_{30}$-TEL$_{10}$**), respectively.

Probing the **PEG-MM**/**iPrSi** copolymerization in more detail, it was found that when greater than 1 equiv of **iPrSi** was used relative to **PEG-MM**, significantly worse results were obtained in terms of the molar mass dispersity (Supplementary Figure 6). Compared to seven- and nine-membered cyclic silyl ether analogs, which yielded copolymers with **PEG-MM** that degraded to form high molecular weight products suggestive of a more gradient or block-like copolymerization, **iPrSi** provided the optimal balance of statistical copolymerization efficiency and synthetic accessibility (Supplementary Figure 7). Density functional theory (DFT) calculations on the structures of cyclic silyl ethers of different ring sizes showed, as expected, that the amount of overall ring strain increased from 7- to 9-

membered silyl ethers although the calculated strain energies are markedly lower than that of norbornene (Supplementary Figure 8); the ability of **iPrSi**, but less so its 7- or 9-membered counterparts, to statistically copolymerize with norbornene derivatives may be dominated by kinetic factors. Lastly, a copolymer of cyclooctene (COE), an eight-membered cyclic olefin monomer commonly used in ROMP, and **PEG-MM** was prepared for comparison to the **iPrSi** copolymer. GPC analysis of this COE-containing copolymer revealed a dramatically broadened molar mass distribution (Supplementary Figure 9), which may be due to differences in the rate of COE homopolymerization or susceptibility to backbiting. Altogether, these results motivated further development of **iPrSi** as a platform for introducing degradable bonds into ROMP-derived copolymers.

Scope of Norbornene Monomers for Copolymerization with iPrSi

Next, the suitability of **iPrSi** for copolymerization with various commonly used norbornene structural motifs, **NB1**-**NB4** (Figure 2a), was explored. Four copolymers $\mathbf{iPrSi_{50}\text{-}NB}x_{\mathbf{50}}$ where x = 1, 2, 3, or 4 were prepared by mixing **NB1**-**NB4** with **iPrSi** in 1:1 ratio followed by addition of 0.02 equivalents (total target DP = 100) of **G3** (Figure 2b). ^{1}H NMR analysis of the crude reaction mixtures (Supplementary Figure 10) revealed good conversion of all monomers in ~30 min. The $\mathbf{iPrSi_{50}\text{-}NB}x_{\mathbf{50}}$ copolymers were analyzed by GPC before and after acidic hydrolysis. In all cases, the addition of **iPrSi** resulted in a modestly broadened molar mass distribution compared to the analogous $\mathbf{NB}x_{\mathbf{50}}$ homopolymer (Figure 2b, see Supplementary Table 1 for molecular weight details). Interestingly, $\mathbf{iPrSi_{50}\text{-}NB1_{50}}$ and $\mathbf{iPrSi_{50}\text{-}NB2_{50}}$ yielded significantly larger fragments after acidic degradation (Figure 2c and 2d, respectively) compared to $\mathbf{iPrSi_{50}\text{-}NB3_{50}}$ and $\mathbf{iPrSi_{50}\text{-}NB4_{50}}$ (Figure 2e and 2f, respectively); $\mathbf{iPrSi_{50}\text{-}NB4_{50}}$ yielded the lowest molecular weight degradation fragments (Figure 2f, blue dashed line). This trend correlates with the expected ROMP reactivity of these norbornene derivatives: **NB1** ~ **NB2** > **NB3** > **NB4**,[28] where relatively slow rates of norbornene homopolymerization correlate with a more statistical incorporation of **iPrSi**. Finally, reactivity ratios of 0.61 and 0.72 were measured for **NB4** and **iPrSi**, respectively, confirming the statistical nature of this copolymerization (Supplementary Figure 11).

Scope of Cyclic Bifunctional Silyl Ethers for Backbone Degradable ROMP Copolymers

The ready availability of different dichlorosilanes should provide a straightforward means to tune the rate of copolymer degradation in this system. As a proof-of-concept, three additional silyl-ether based monomers: **MeSi**, **EtSi**, and **PhSi** (Figure 3a) were prepared following similar procedures for the synthesis of **iPrSi** (Supplementary Scheme 1). Copolymerizations of these monomers with **PEG-MM** (Figure 1b, total target DP = 60) provided a series of bottlebrush copolymers $\mathbf{\mathit{R}Si_{30}\text{-}PEG_{30}}$ (Figure 3b; R = Me, Et, Ph, or iPr); regardless of the silyl ether monomer used, the copolymers displayed low dispersities as determined by GPC ($Đ$ = 1.02 to 1.24 with slightly higher dispersities observed for smaller silyl ether substituents; Figure 3c). Moreover, ^{1}H NMR analysis of the crude reaction mixtures showed high monomer conversion (Supplementary Figures 12–13), suggesting copolymer formation. Finally, acidic hydrolysis led to degradation of $\mathbf{\mathit{R}Si_{30}\text{-}PEG_{30}}$ copolymers with no degradation of the homopolymer $\mathbf{PEG_{30}}$ (Figure 3d).

The hydrolysis kinetics of ***R*Si$_{30}$-PEG$_{30}$** were studied as a function of pH. Key to these experiments was the high solubility of the copolymers in aqueous media (>25 mg/mL). Each sample was incubated in phosphate/citrate buffers (5 mg of copolymer / mL; pH 5.5, 6.5, or 7.4) at 37 °C; samples were taken at various time points, dried, and analyzed by GPC (see Supplementary Information, Supplementary Figure 14). Example GPC traces depicting the extent of degradation of **iPrSi$_{30}$-PEG$_{30}$** as a function of time at pH = 6.5 and after 35 d at various pH values are provided in Figures 4a and 4b, respectively. Notably, even at mildly acidic pH values (5.5 and 6.5) significant degradation is observed over the course of 35 d. The extent of degradation for each ***R*Si$_{30}$-PEG$_{30}$** sample versus time in pH 5.5 buffer was quantified by integration of the corresponding GPC traces (Figure 4c); the relative extents of degradation versus time followed the expected reactivity trends of these silyl ether functional groups.[29,30] Interestingly, the copolymer peaks in the GPC traces shifted to only slightly longer retention times at early time points with the concomitant appearance of new peaks corresponding to degradation products, which suggests that the degradation begins from the more accessible bottlebrush backbone chain ends and proceeds inwardly, which agrees well with the reported regioselective reactivity of bottlebrush polymers.[31,32] Altogether, the four silyl ether monomers described here allow us to readily tune the degradation percentage of bottlebrush copolymers over four orders-of-magnitude at physiologically relevant pH values. It should be noted that although these bottlebrush copolymers degrade under aqueous conditions, they are stable for at least two months in organic solvents at room temperature (e.g., dioxane) (Supplementary Figure 15), which enables the facile synthesis and handling until they are ready to be deployed for an application of interest.

Chain transfer via backbiting represents a potential mechanism for increased dispersity and loss of molecular weight control in ROMP. To investigate the potential role of chain transfer in this system, ***R*Si$_{50}$-NB3$_{50}$** samples were incubated for 1 h with the chain transfer agent *cis*-4-octene in the presence of Grubbs 2nd-generation catalyst. The GPC traces of the samples with smaller Si substituents, **MeSi$_{50}$-NB3$_{50}$** and **EtSi$_{50}$-NB3$_{50}$**, showed small shifts to shorter retention times, indicative of a minor decrease in molecular size (Supplementary Figure 16). The GPC traces for the samples with larger substituents, on the other hand, were essentially unchanged during the course of this experiment.[33] These results suggest that the ***R*Si$_{50}$-NB3$_{50}$** polymer backbones are largely resistant to chain transfer reactions, which stands in contrast to analogous copolymers of norbornene derivatives with cyclooctene.[34,35]

Application of iPrSi for Regioselective Polymer and Nanoparticle Degradation.

The ability to install degradable bonds into polynorbornene backbones could open avenues for regioselective degradation of multiblock polymers and complex macromolecular architectures. To demonstrate this concept, a DP = 100 diblock copolymer **NB4$_{50}$-*b*-(iPrSi$_{50}$-NB4$_{50}$)** featuring one block of **NB4** and a second block of statistically copolymerized **NB4** and **iPrSi** was prepared via sequential ROMP. GPC traces of **NB4$_{50}$-*b*-(iPrSi$_{50}$-NB4$_{50}$)** before and after acidic hydrolysis (Supplementary Figure 17) suggest that degradation only occurred in one block: a polymeric degradation product with a similar retention time to that of a control **NB4$_{50}$** homopolymer was observed.

Applying a similar approach in the context of bottlebrush polymers, a diblock bottlebrush copolymer **PEG$_{30}$-*b*-(iPrSi$_{30}$-PS$_{30}$)** featuring a PEG-based block and a degradable PS-based block was prepared. Acidic hydrolysis yielded a polymeric species with a nearly identical retention time to a **PEG$_{30}$** bottlebrush homopolymer and degraded fragments of the PS block (Supplementary Figure 18). Switching the location of **iPrSi** from the PS block to the PEG block by polymerizing **PS-MM** first and then a mixture of **PEG-MM** and **iPrSi** enabled selective degradation of the latter block (Supplementary Figure 18), providing proof-of-concept for regioselective degradation of blocks of choice in a multiblock bottlebrush copolymer.

The installation of degradable bonds into the block junction of a multi-block copolymer can be used to trigger interesting self-assembly behaviors.[36–38] To demonstrate this concept in the context of bottlebrush block copolymers, a triblock bottlebrush **PEG$_{30}$-*b*-(iPrSi$_{10}$-NB3$_{20}$)-*b*-PS$_{60}$** featuring a **PEG-MM**, a statistical block of 1:1 **iPrSi** and **NB4**, and a block of **PS-MM** was prepared. A control sample, **PEG$_{30}$-*b*-(NB3$_{20}$)-*b*-PS$_{60}$**, lacking **iPrSi** in the center block was also prepared. GPC analysis (Supplementary Figure 19) revealed that only the **iPrSi** containing copolymer degraded into two halves upon treatment with HCl. Upon dissolution of these triblock copolymers in methanol, which is a selective solvent for the PEG block, we observed that both samples formed translucent solutions indicative of assembly into larger aggregates (Supplementary Figure 19). Addition of 0.1% v/v of 2 M HCl led to precipitation of the silyl ether containing sample and not the control, presumably due to cleavage of the central block of the former releasing the PEG block and subsequent aggregation of the methanol-insoluble PS bottlebrush polymers. Though these results are preliminary, they hint at the potential of such systems for applications in self-assembly with triggered shedding of one block versus another.

Extending to star-like architectures, the crosslinking of living bottlebrush polymers with bis-norbornenes is a useful strategy for the synthesis of brush-arm star polymers (BASPs) with degradable nanogel cores.[25,39–41] To determine if silyl ether monomers could be used to impart shell degradability to BASPs, as well as distinct core and shell degradation rates, a series of living bottlebrush polymers **MeSi$_7$-PEG$_7$**, **EtSi$_7$-PEG$_7$**, and **iPrSi$_7$-PEG$_7$** were crosslinked with 20 equiv of bis-norbornene acetal **AcXL** to provide ***R*Si-BASPs** (where *R* = Me, Et, or iPr, respectively, Figure 5a).[39] These three BASPs had similar GPC peak shapes compared to a traditional BASP prepared using only **PEG-MM** and **AcXL** (Figure 5b). Upon treatment with trifluoroacetic acid, a strong acid, the BASP lacking silyl ethers in its shell underwent acetal core degradation to provide the corresponding **PEG$_7$** bottlebrush polymer products. Under the same conditions, the ***R*Si-BASP**s yielded significantly smaller fragments due to both acetal core and ***R*Si$_7$-PEG$_7$** shell degradation (Figure 5a and 5b).

To assess the degradation of ***R*Si-BASP**s under physiologically relevant conditions, solutions of these copolymers in phosphate/citrate buffers (pH 5.0 or pH 7.4) were held at room temperature; degradation as a function of time was measured by dynamic light scattering (Figure 5c, Supplementary Figure 20). The traditional BASP lacking silyl ethers showed virtually no change in its hydrodynamic diameter under these conditions, which supports previous reports that the acetal core of similar BASPs is stable under neutral and mildly acidic aqueous media.[17,39] In contrast, the ***R*Si-BASP**s aggregated at rates that increased

with pH and correlated with the silyl ether reactivity, which is attributed to degradation of the silyl-ether containing bottlebrush shell and exposure of the hydrophobic acetal core (Figure 4a). GPC analysis of the **EtSi-BASP** treated under these conditions confirmed that they did indeed degrade to a significant extent after 96 h at pH 5.0 (Supplementary Figure 21). Notably, the extents of degradation for ***R*Si-BASP**s were significantly less (>10-fold) than those for the corresponding bottlebrush polymers after the same amount of time: *e.g.*, **MeSi-Brush** showed almost instantaneous degradation at pH 7.4 while **MeSi-BASP** remained intact for 12 h. These results highlight the differences in steric shielding between small bottlebrush polymers and their larger BASP counterparts, agreeing well with previous reports on the stability of nitroxide radicals covalent attached to these polymer architectures.[40,41]

Biological Applications of Degradable Bottlebrush Copolymers

We sought to determine if the installation of silyl ethers into the backbone of PEGylated bottlebrush polymers could influence their performance as biomaterials. Cy3-labeled samples of **MeSi$_{30}$-PEG$_{30}$**, **EtSi$_{30}$-PEG$_{30}$**, **iPrSi$_{30}$-PEG$_{30}$**, **PhSi$_{30}$-PEG$_{30}$** and a control **PEG$_{30}$** lacking silyl ethers (Supplementary Figure 22) were incubated with OVCAR8 and Jurkat cells for 36 h; cell viability was assessed by flow cytometry (Supplementary Figure 23). All of the samples showed minimal cytotoxicity at the concentration tested (1 mg/mL). A noticeable increase in cell uptake was observed for the samples containing **iPrSi** and **PhSi** compared to the control sample (Supplementary Figure 24). Though the origin of this result is under investigation and does not appear to be due to differences in subcellular localization (Supplementary Figure 25), hinting at the possibility of tuning cell uptake in this system using simple copolymerization strategies.

We hypothesized that **iPrSi$_{30}$-PEG$_{30}$** and **PhSi$_{30}$-PEG$_{30}$**, which have degradation half-lives at pH 6.5 of ~6 weeks and ~2 weeks, respectively, would display early-stage biodistribution (BD) and pharmacokinetic (PK) profiles that are similar to their non-silyl ether based PEG bottlebrush polymer counterpart[12]; they may, however, show increased long-term clearance as a result of their degradability. To test this hypothesis, 5 mg of each Cy5.5-labeled version of **iPrSi$_{30}$-PEG$_{30}$**, **PhSi$_{30}$-PEG$_{30}$** and **PEG$_{30}$** (control) (Supplementary Figure 22) dissolved in 5% aqueous glucose were administered via tail-vein injection to female BALB/c mice (n = 3 for short-term PK/BD studies; n = 4 for long-term clearance studies). The mice were sacrificed at various time points and the percentage of injected dose of Cy5.5 in blood for each polymer was determined via fluorescence spectroscopy. All of the polymers showed similar and typical two-phase clearance profiles over the first 72 h (Figure 6a). In contrast, there was ~6-fold less (P < 0.01) of the silyl-ether containing bottlebrush copolymers (**iPrSi$_{30}$-PEG$_{30}$** and **PhSi$_{30}$-PEG$_{30}$**) in circulation at the three-week and six-week timepoints compared to the non-degradable control (Figure 6b). These data suggest that the installation of silyl ethers into the backbone of these polymers has little effect on their short-term PK, but significantly enhances their long-term clearance from the blood compartment.

The BD of these polymers as a function of time (from 72 h to 10 weeks) was assessed by fluorescence analysis of tissue homogenates. As is often the case for PEG-based materials,[42]

significant early accumulation was observed in the liver and spleen (Figure 6c, Supplementary Figures 26–27); the extent of accumulation was similar for all three polymers after 72 hours. Strikingly, after 3 weeks, significantly lower amounts of Cy5.5 fluorescence were observed in the livers ($P < 0.01$) and spleens ($P < 0.01$) of animals administered the silyl-ether containing copolymers.[43,44] After 10 weeks, the liver signals were similar for both the control and the silyl-ether bottlebrush polymers; the latter, however, continued to show much lower splenic accumulation ($P < 0.01$). Blood chemistry (Supplementary Figure 28) as well as liver, spleen, and kidney histopathology (Supplementary Figure 29) revealed mild hyperglycemia but otherwise no discernable toxicities for the control bottlebrush and its silyl-ether analogues. Though the mechanisms of degradation for biomaterials *in vivo* can be complicated, and other factors in addition to degradability such as differential cell uptake and/or protein corona formation may explain the observed differences in *in vivo* behaviors for these bottlebrush copolymers, these proof-of-principle results hint at the potential for using silyl ether monomers to tune the *in vivo* PK and BD of biocompatible ROMP-based copolymers.

Conclusions

In summary, we report that 8-membered cyclic silyl-ether-based olefins copolymerize efficiently with a wide variety of norbornene-based (macro)monomers via ROMP rendering these widely used polymers degradable. By tuning the silyl ether substituents, the extent of degradation as a function of time can be tuned over several orders of magnitude with minimal impact on copolymerization control. Proofs-of-principle for how this approach can enable regioselective degradation of multi-block bottlebrush and BASP macromolecular architectures are provided. In addition, the impact of degradability on the *in vitro* and *in vivo* biological performance of PEG-based bottlebrush copolymers is assessed, showing that these monomers can be used to enhance long-term tissue clearance. These results will enable applications of ROMP-derived polymers in triggered self-assembly, stimuli-responsive materials, sustainability, and biomedicine.

Supplementary Material

Refer to Web version on PubMed Central for supplementary material.

Acknowledgements

The authors thank the National Institutes of Health (1R01CA220468-01) for support of this work. P.S. was supported by a fellowship from the American Cancer Society. H.V.-T.N was supported by the National Science Foundation (Graduate Research Fellowship).

References

1. Mortell KH, Weatherman RV & Kiessling LL Recognition specificity of neoglycopolymers prepared by ring-opening metathesis polymerization. J. Am. Chem. Soc. 118, 2297–2298 (1996).
2. Kiessling LL, Gestwicki JE & Strong LE Synthetic multivalent ligands as probes of signal transduction. Angew. Chemie - Int. Ed. 45, 2348–2368 (2006).
3. Blum AP et al. Peptides displayed as high density brush polymers resist proteolysis and retain bioactivity. J. Am. Chem. Soc. 136, 15422–15437 (2014). [PubMed: 25314576]

4. James CR et al. Poly(oligonucleotide). J. Am. Chem. Soc. 136, 11216–11219 (2014). [PubMed: 25077676]
5. Buchmeiser MR, Sinner F, Mupa M & Wurst K Ring-opening metathesis polymerization for the preparation of surface-grafted polymer supports. Macromolecules 33, 32–39 (2000).
6. Rule JD & Moore JS ROMP reactivity of endo- and exo-dicyclopentadiene. Macromolecules 35, 7878–7882 (2002).
7. Kalow JA & Swager TM Synthesis of Miktoarm Branched Conjugated Copolymers by ROMPing in and Out. ACS Macro Lett. 4, 1229–1233 (2015). [PubMed: 26523242]
8. Xia Y, Olsen BD, Kornfield JA & Grubbs RH Efficient Synthesis of Narrowly Dispersed Brush Copolymers and Study of Their Assemblies: The Importance of Side Chain Arrangement. J. Am. Chem. Soc. 131, 18525–18532 (2009). [PubMed: 19947607]
9. Johnson JA et al. Drug-Loaded, Bivalent-Bottle-Brush Polymers by Graft-through ROMP. Macromolecules 43, 10326–10335 (2010). [PubMed: 21532937]
10. Johnson JA et al. Core-Clickable PEG- Branch -Azide Bivalent-Bottle-Brush Polymers by ROMP: Grafting-Through and Clicking-To. J. Am. Chem. Soc. 133, 559–566 (2011). [PubMed: 21142161]
11. Liu J et al. 'Brush-first' method for the parallel synthesis of photocleavable, nitroxide-labeled poly(ethylene glycol) star polymers. J. Am. Chem. Soc. 134, 16337–16344 (2012). [PubMed: 22953714]
12. Sowers MA et al. Redox-responsive branched-bottlebrush polymers for in vivo MRI and fluorescence imaging. Nat. Commun. 5, 5460 (2014). [PubMed: 25403521]
13. Kawamoto K et al. Graft-through Synthesis and Assembly of Janus Bottlebrush Polymers from A-Branch -B Diblock Macromonomers. J. Am. Chem. Soc. 138, 11501–11504 (2016). [PubMed: 27580971]
14. Cheng L-C et al. Templated Self-Assembly of a PS- Branch -PDMS Bottlebrush Copolymer. Nano Lett. 18, 4360–4369 (2018). [PubMed: 29877712]
15. Rokhlenko Y, Kawamoto K, Johnson JA & Osuji CO Sub-10 nm Self-Assembly of Mesogen-Containing Grafted Macromonomers and Their Bottlebrush Polymers. Macromolecules 51, 3680–3690 (2018).
16. Guo Z-H et al. Janus Graft Block Copolymers: Design of a Polymer Architecture for Independently Tuned Nanostructures and Polymer Properties. Angew. Chemie Int. Ed. 57, 8493–8497 (2018).
17. Golder MR et al. Reduction of liver fibrosis by rationally designed macromolecular telmisartan prodrugs. Nat. Biomed. Eng. 2, 822–830 (2018). [PubMed: 30918745]
18. Fishman JM & Kiessling LL Synthesis of Functionalizable and Degradable Polymers by Ring-Opening Metathesis Polymerization. Angew. Chemie Int. Ed. 52, 5061–5064 (2013).
19. Gutekunst WR & Hawker CJ A General Approach to Sequence-Controlled Polymers Using Macrocyclic Ring Opening Metathesis Polymerization. J. Am. Chem. Soc. 137, 8038–8041 (2015). [PubMed: 26053158]
20. Mallick A et al. Oxadiazabicyclooctenone as a versatile monomer for the construction of pH sensitive functional polymers via ROMP. Polym. Chem. 9, 372–377 (2018).
21. Moatsou D, Nagarkar A, Kilbinger AFM & O'Reilly RK Degradable precision polynorbornenes via ring-opening metathesis polymerization. J. Polym. Sci. Part A Polym. Chem. 54, 1236–1242 (2016).
22. Yasir M, Liu P, Tennie IK & Kilbinger AFM Catalytic living ring-opening metathesis polymerization with Grubbs' second- and third-generation catalysts. Nat. Chem. 11, 488–494 (2019). [PubMed: 30962611]
23. Parrott MC et al. Tunable Bifunctional Silyl Ether Cross-Linkers for the Design of Acid-Sensitive Biomaterials. J. Am. Chem. Soc. 132, 17928–17932 (2010). [PubMed: 21105720]
24. Szychowski J et al. Cleavable biotin probes for labeling of biomolecules via azide-alkyne cycloaddition. J. Am. Chem. Soc. 132, 18351–18360 (2010). [PubMed: 21141861]
25. Shibuya Y, Nguyen HV-T & Johnson JA Mikto-Brush-Arm Star Polymers via Cross-Linking of Dissimilar Bottlebrushes: Synthesis and Solution Morphologies. ACS Macro Lett. 6, 963–968 (2017).

26. Sveinbjornsson BR et al. Rapid self-assembly of brush block copolymers to photonic crystals. Proc. Natl. Acad. Sci. 109, 14332–14336 (2012). [PubMed: 22912408]
27. Golder MR et al. Reduction of liver fibrosis by rationally designed macromolecular telmisartan prodrugs. Nat. Biomed. Eng. 2, 822–830 (2018). [PubMed: 30918745]
28. Radzinski SC, Foster JC, Chapleski RC, Troya D & Matson JB Bottlebrush Polymer Synthesis by Ring-Opening Metathesis Polymerization: The Significance of the Anchor Group. J. Am. Chem. Soc. 138, 6998–7004 (2016). [PubMed: 27219866]
29. Gillard JW et al. Symmetrical Alkoxysilyl Ethers. A New Class of Alcohol-Protecting Groups. Preparation of tert-Butoxydiphenylsilyl Ethers. J. Org. Chem. 53, 2602–2608 (1988).
30. Davies JS, Higginbotham CL, Tremeer EJ, Brown C & Treadgold RC Protection of hydroxy groups by silylation: use in peptide synthesis and as lipophilicity modifiers for peptides. J. Chem. Soc. Perkin Trans. 1 3043 (1992). doi:10.1039/p19920003043
31. Xia Y et al. EPR Study of Spin Labeled Brush Polymers in Organic Solvents. J. Am. Chem. Soc. 133, 19953–19959 (2011). [PubMed: 22023139]
32. Burts AO et al. Using EPR To Compare PEG- branch -nitroxide “Bivalent-Brush Polymers” and Traditional PEG Bottle–Brush Polymers: Branching Makes a Difference. Macromolecules 45, 8310–8318 (2012).
33. Elling BR & Xia Y Living Alternating Ring-Opening Metathesis Polymerization Based on Single Monomer Additions. J. Am. Chem. Soc. 137, 9922–9926 (2015). [PubMed: 26182144]
34. Alonso-Villanueva J et al. ROMP of Functionalized Cyclooctene and Norbornene Derivatives and their Copolymerization with Cyclooctene. J. Macromol. Sci. Part A 48, 211–218 (2011).
35. Gringolts ML et al. Synthesis of norbornene–cyclooctene copolymers by the cross-metathesis of polynorbornene with polyoctenamer. RSC Adv. 5, 316–319 (2015).
36. Bang J et al. Defect-free nanoporous thin films from ABC triblock copolymers. J. Am. Chem. Soc. 128, 7622–7629 (2006). [PubMed: 16756319]
37. Zhao H, Sterner ES, Coughlin EB & Theato P o -Nitrobenzyl Alcohol Derivatives: Opportunities in Polymer and Materials Science. Macromolecules 45, 1723–1736 (2012).
38. Zhang W et al. Tuning microdomain spacing with light using ortho-nitrobenzyl-linked triblock copolymers. J. Polym. Sci. Part B Polym. Phys. 56, 355–361 (2018).
39. Gao AX, Liao L & Johnson JA Synthesis of Acid-Labile PEG and PEG-Doxorubicin-Conjugate Nanoparticles via Brush-First ROMP. ACS Macro Lett. 3, 854–857 (2014). [PubMed: 25243099]
40. Nguyen HV-T et al. Nitroxide-Based Macromolecular Contrast Agents with Unprecedented Transverse Relaxivity and Stability for Magnetic Resonance Imaging of Tumors. ACS Cent. Sci. 3, 800–811 (2017). [PubMed: 28776023]
41. Nguyen HV-T et al. Triply Loaded Nitroxide Brush-Arm Star Polymers Enable Metal-Free Millimetric Tumor Detection by Magnetic Resonance Imaging. ACS Nano 12, 11343–11354 (2018). [PubMed: 30387988]
42. Li S-D & Huang L Pharmacokinetics and Biodistribution of Nanoparticles. Mol. Pharm. 5, 496–504 (2008). [PubMed: 18611037]
43. Demoy M et al. Splenic Trapping of Nanoparticles: Complementary Approaches for In Situ Studies. Pharm. Res. 14, 463–468 (1997). [PubMed: 9144732]
44. Cataldi M, Vigliotti C, Mosca T, Cammarota M & Capone D Emerging Role of the Spleen in the Pharmacokinetics of Monoclonal Antibodies, Nanoparticles and Exosomes. Int. J. Mol. Sci. 18, (2017).

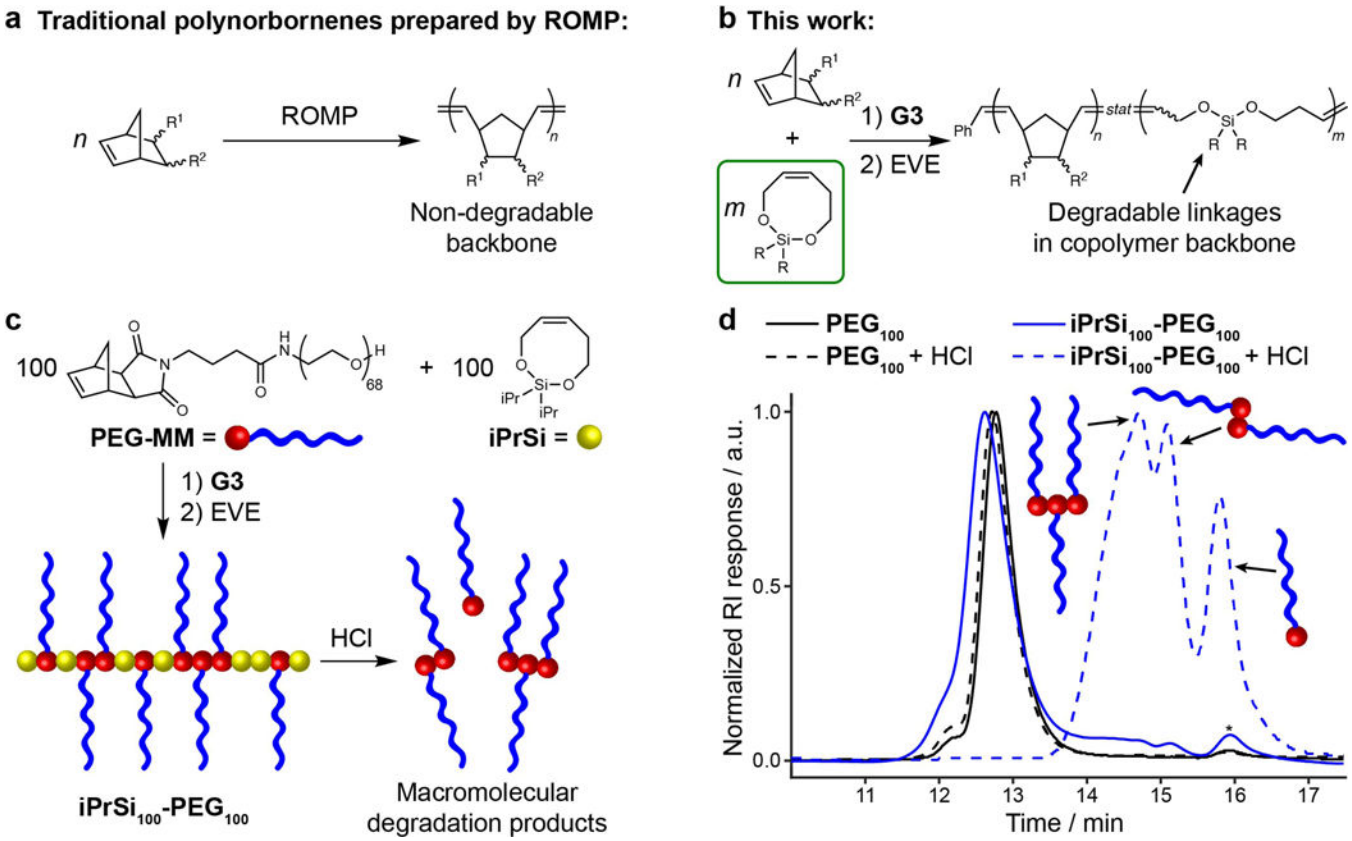

Figure 1. Study design and initial results.

a. Polynorbornenes prepared via ROMP feature an all-carbon backbone, preventing their facile hydrolytic degradation. **b.** Proposed approach for introducing degradable segments into ROMP copolymers via copolymerization with 8-membered ring bifunctional silyl-ether-based olefins. **G3** = Grubbs 3rd-generation bispyridyl complex. EVE = ethyl vinyl ether. **c.** Synthetic scheme for the synthesis of backbone-degradable PEG-based bottlebrush polymer (**iPrSi$_{100}$-PEG$_{100}$**) derived from copolymerization of a norbornene-terminated polyethylene glycol macromonomer (**PEG-MM**) with an eight-membered cyclic bifunctional silyl ether monomer (**iPrSi,** 1:1 molar ratio of monomers). Acidic degradation cleaves the polynorbornene backbone leading to the production of oligomeric PEG-based fragments. **d.** GPC traces before and after forced hydrolysis of **iPrSi$_{100}$-PEG$_{100}$** and a traditional PEG bottlebrush homopolymer (**PEG$_{100}$**) demonstrating that only the copolymer undergoes degradation. *indicates residual **PEG-MM** from the ROMP reaction.

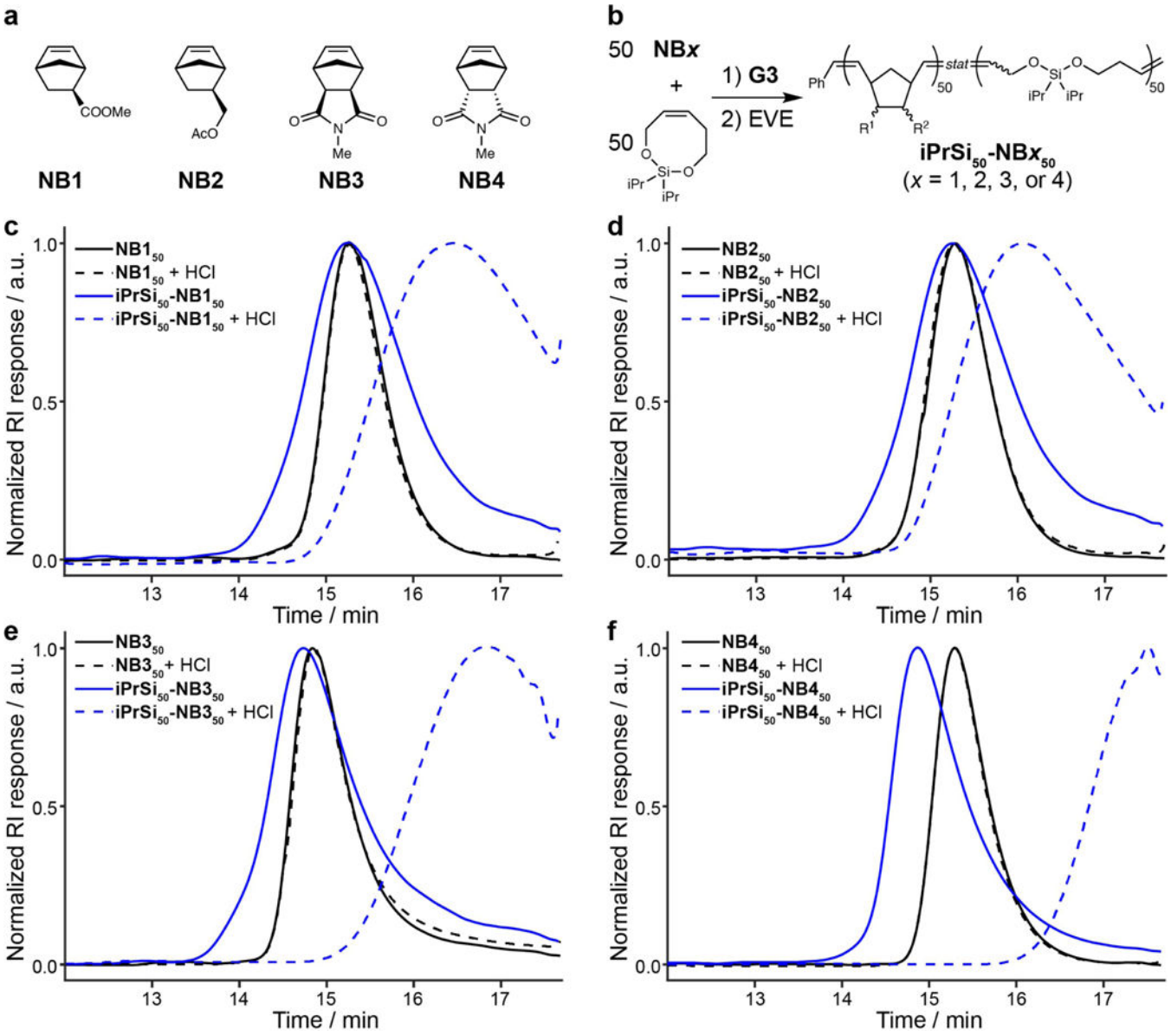

Figure 2. Norbornene monomer scope.

a. Library of small-molecule norbornene derivatives **NB1**-**NB4** with varying ROMP propagation rates used to investigate the scope of copolymerization with **iPrSi**. **b.** General synthetic scheme for the synthesis of copolymers of **NB*x*** and **iPrSi** (**iPrSi$_{50}$-NB*x*$_{50}$**). **c.** GPC traces for copolymers of **iPrSi** and **NB1**. **d.** GPC traces for copolymers of **iPrSi** and **NB2**. **e.** GPC traces for copolymers of **iPrSi** and **NB3**. **f.** GPC traces for copolymers of **iPrSi** and **NB4**. All of the copolymers degrade under acidic conditions, whereas homopolymers of **NB1**-**NB4** do not. Moreover, the size of the degradation products correlates with the monomer reactivity, with the least reactive monomer **NB4** yielding the smallest degradation products.

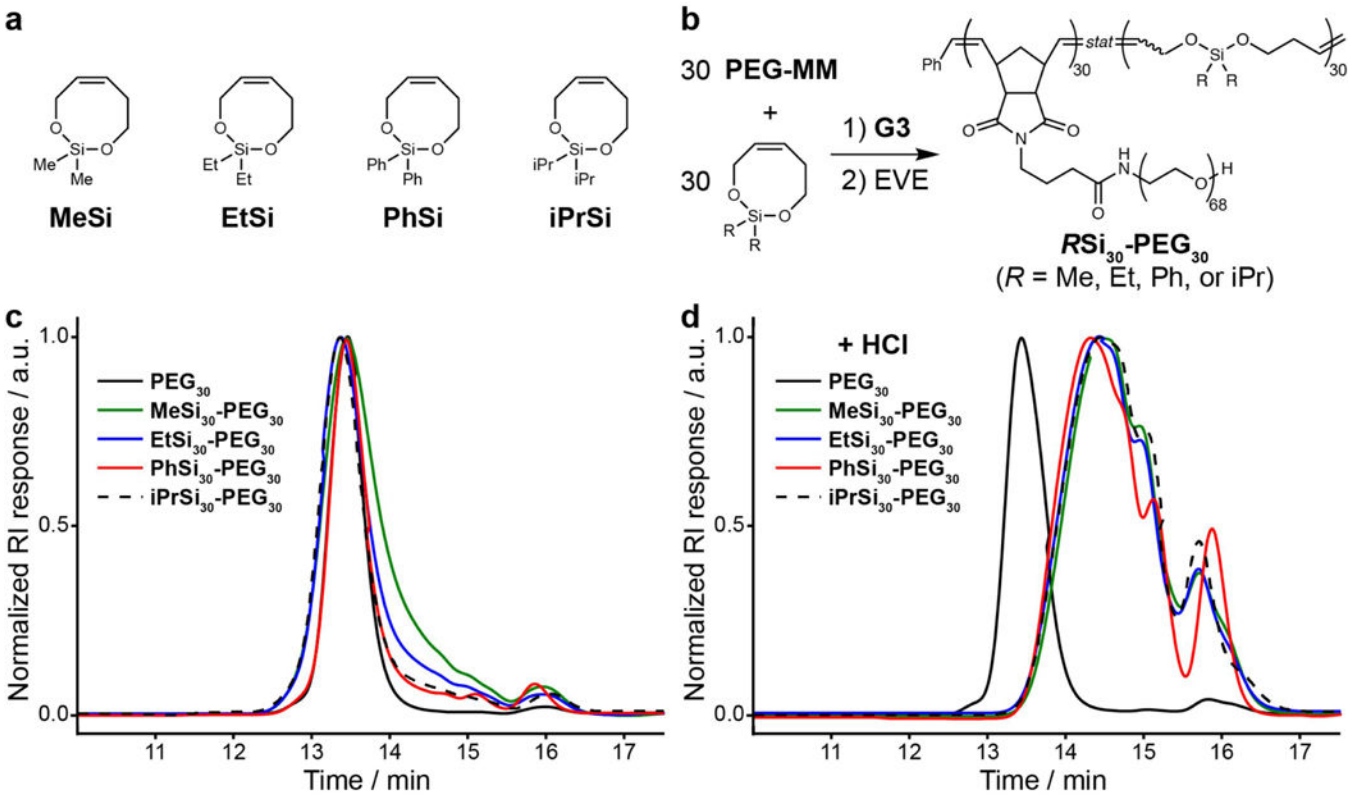

Figure 3. Bifunctional silyl ether monomer scope.

a. Library of bifunctional silyl ether monomers with varied Si substituents that ultimately dictate the polymer degradation rate. **b.** General synthetic scheme for the synthesis of copolymers of ***R*Si** and **PEG-MM** (***R*Si$_{30}$-PEG$_{30}$**). **c.** GPC traces showing the successful formation of bottlebrush copolymers using the four different silyl ether monomers and **PEG-MM**. **d.** GPC traces showing the degradation products of the four copolymers as well as **PEG$_{30}$**. The homopolymer **PEG$_{30}$** is not degradable under these conditions, while the copolymers are.

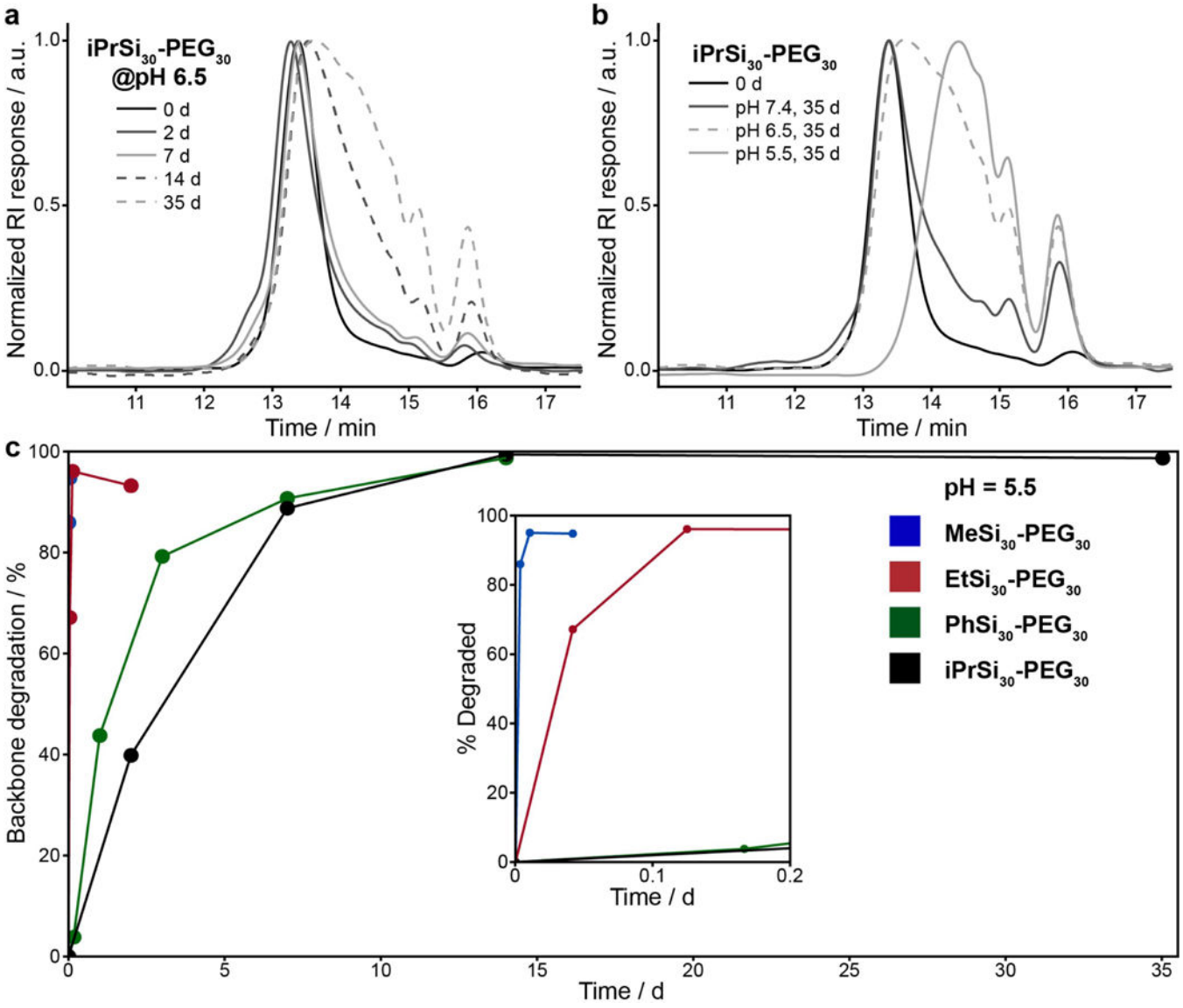

Figure 4. Bottlebrush copolymer degradation studies as a function of time, pH, and bifunctional silyl ether composition.

a. GPC traces for **iPrSi$_{30}$-PEG$_{30}$** incubated at pH 6.5 for times ranging from 0 to 35 d. **b.** GPC traces for **iPrSi$_{30}$-PEG$_{30}$** incubated at pH values from 5.5 to 7.4 for 35 d. At pH 7.4, little degradation occurs within 35 d, whereas at pH 5.5 degradation to small products is complete. c. Percentage of backbone degradation as a function of time for the ***R*Si$_{30}$-PEG$_{30}$** series of bottlebrush copolymers incubated at pH 5.5. The extent of degradation varies with the silyl ether substituents.

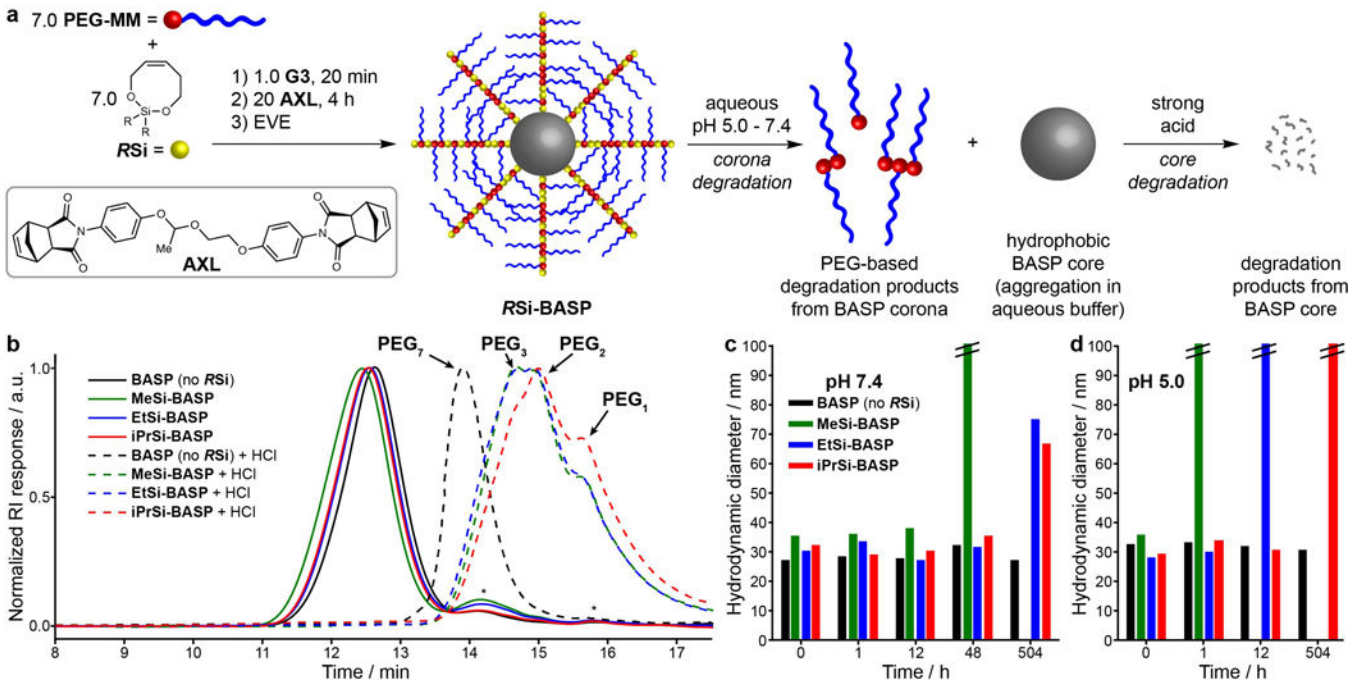

Figure 5. Regioselective degradation of bifunctional silyl-ether containing brush-arm star polymers (BASPs).

a. Synthesis of BASPs via crosslinking of short (DP = 7) PEG-based bottlebrush (co)polymers with **AcXL**. When a silyl ether monomer is combined with **PEG-MM** in the first step, the resulting BASPs (***R*Si-BASP**) have silyl-ether linkages (yellow) with substituents *R* in the backbones of their bottlebrush arms. In addition, they have acetal cores (grey) that can be independently degraded due to their different susceptibility to acid. b. GPC traces showing the successful formation of BASPs without silyl ethers (**BASP**, black curve) or with (***R*Si-BASP**, all other solid curves). Forcing acidic hydrolysis only cleaves the core of the **BASP** (lacking silyl ethers) re-generating the DP = 7 bottlebrush arms (black dashed line). In contrast, ***R*Si-BASP**s undergo both core and arm degradation yielding significantly smaller fragments. *indicates residual bottlebrush (left) and **PEG-MM** (right) following the ROMP reaction. **c.** Hydrodynamic diameters of ***R*Si-BASP**s as a function of time when incubated at pH 7.4. A sharp increase in hydrodynamic diameter is indicative of degradation of the silyl-ether bottlebrush shell, which exposes the hydrophobic acetal-based core that is not degradable under these mild conditions, leading to aggregation. **d.** Hydrodynamic diameters of ***R*Si-BASP**s as a function of time when incubated at pH 5.0. As observed for the bottlebrush copolymers, the silyl ether substituents (*R*) dictate the extent of degradation of RSi-BASPs as a function of time at a given pH.

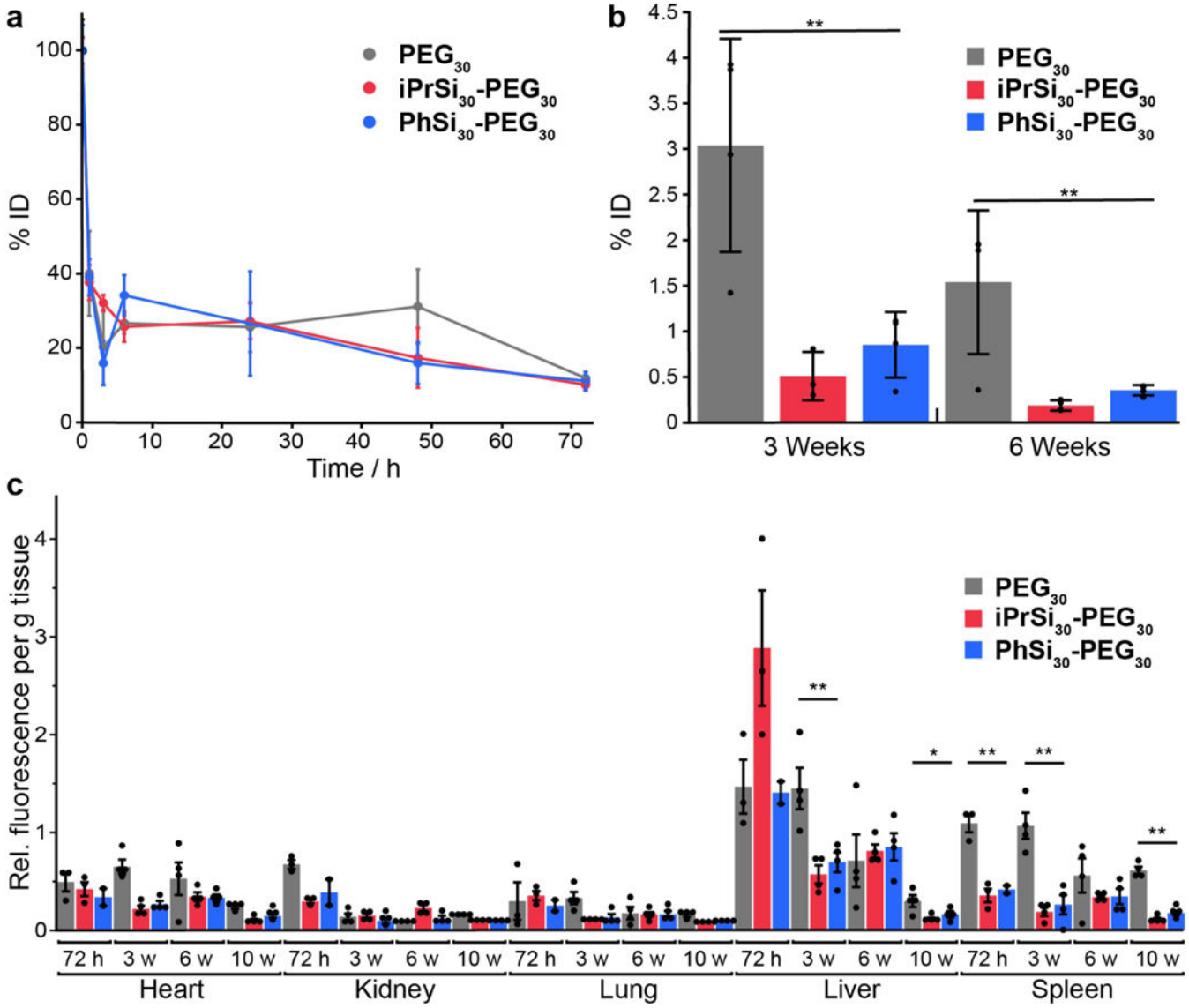

Figure 6. Biological studies of fluorescently labeled bottlebrush (co)polymers.

a. 72 h pharmacokinetics (PK) as determined by fluorescence analysis of blood samples. No significant differences between the silyl ether-containing bottlebrush copolymers and their homopolymer analogue were observed (n = 3 mice/timepoint, mean/S.D.). **b.** In contrast to short-term PK, significantly lower amounts of the silyl ether-containing bottlebrush copolymers are present in circulation after 3 weeks and 6 weeks. Statistical significance was assessed by a two-tailed Student's t-test. (n = 3 mice/timepoint, mean/S.D.) ** - $p < 0.01$. **c.** Concentrations of bottlebrush polymers with and without silyl ether comonomers in various organs as a function of time from three days to ten weeks after injection. The silyl ether-containing bottlebrush polymers showed a lower signal in the liver and especially the spleen over the course of the experiment. Statistical significance was assessed by a two-tailed Student's t-test. (n = 3 mice at 72 h, 4 mice at 3, 6, and 10 w, mean/S.D.) * - $p < 0.05$, ** - $p < 0.01$.